Journal of Applied Fluid Mechanics, Vol. 8, No. 4, pp. 803-813, 2015.
Available online at www.jafmonline.net, ISSN 1735-3572, EISSN 1735-3645.
DOI: 10.18869/acadpub.jafm.73.238.22995

Mixed Convection Flow of Casson Nanofluid over a Stretching Sheet with Convectively Heated Chemical Reaction and Heat Source/Sink

T. Hayat[1,2], M. Bilal Ashraf [3†], S. A. Shehzad[4] and A. Alsaedi[2]

[1]*Department of Mathematics, Quaid-i-Azam University 45320 Islamabad 44000, Pakistan*
[2]*Nonlinear Analysis and Applied Mathematics (NAAM) Research Group, Faculty of Science, King Abdulaziz University, P. O. Box 80203, Jeddah 21589, Saudi Arabia*
[3]*Department of Mathematics, Comsats Institute of Information Technology, Wah Cantt, Pakistan*
[4]*Department of Mathematics, Comsats Institute of Information Technology, Sahiwal 57000, Pakistan*

†*Corresponding Author Email: bilalashraf_qau@yahoo.com*

(Received May 8, 2014; accepted July 16, 2014)

ABSTRACT

The present study addresses the mixed convection flow of non-Newtonian nanofluid over a stretching surface in presence of thermal radiation, heat source/sink and first order chemical reaction. Casson fluid model is adopted in the present study. Magnetic field contribution is incorporated in the momentum equation whereas the aspects of nanoparticles are considered in the energy and concentration equations. Convective boundary conditions for both heat and mass transfer are utilized. Similarity transformations are employed to reduce the partial differential equations into ordinary differential equations. Series solutions of the resulting problem are obtained. Impacts of all the physical parameters on the velocity, temperature and concentration fields are analyzed graphically. Numerical values of different involved parameters for local skin friction coefficient, local Nusselt and Sherwood numbers are obtained and discussed.

Keywords: Casson nanofluid; Mixed convection flow; Thermal radiation; Magnetic field; Chemical reaction; Heat source/sink.

NOMENCLATURE

u, v and w	velocity components	M	Hartman number
p_y	yield stress of fluid	R	radiation parameter
k_e	mean absorption coefficient	N_b	Brownian motion parameter
c^*	specific heat of nanoparticles		
D_B	brownian diffusion coefficient	β_T	thermal expansion coefficient
T_f and C_f	hot fluid temperature and concentration	σ^*	electrical conductivity
Gr_x	The local Grashof number	ρ	density of fluid
Pr	Prandtl number	ν	kinematic viscosity
N_t	thermophoretic parameter	ρ^*	density of nanoparticles
B_0	applied magnetic field	λ	mixed convection parameter
g	gravitational acceleration	β	casson fluid parameter
Q	heat generation/absorption	β_C	concentration expansion coefficient
h and h^*	heat and mass transfer coefficients	σ	thermal diffusivity
N	concentration buoyancy	ν	kinematic viscosity

σ_s	Stefan-Boltzmann constant	β_1	heat source/sink parameter
γ_1	Heat transfer Biot number	γ_2	Mass transfer Biot number

1. INTRODUCTION

Now a days, the energy efficiency is an extremely important topic in view of thermal conductivity enhancement amongst the researchers. For this purpose the researchers considered the involvement of nanoparticles in the base fluid. Originally Masuda et al. (1996) reported the liquid dispersions of submicron particles or nanoparticles. After that, first time nanofluid term is used by Choi (1995). In comparison to the base fluids, thermal conductivity of nanofluid is too high that's why these have been used in many energetic systems such as cooling of nuclear systems, radiators, natural convection in enclosures etc. The model proposed by Buongiorno (2006) studies the Brownian motion and the thermophoresis on the heat transfer characteristics. Recently, the analytical solutions for the laminar axisymmetric mixed convection boundary layer nanofluid flow past a vertical cylinder is obtained by Rashidi et al. (2012a). Stagnation point flow of nanofluid near a permeable stretched surface with thermal convective condition is provided by Alseadi et al. (2012). Mustafa et al. (2013) discussed the boundary layer flow of nanofluid over an exponentially stretching sheet with convective boundary conditions. Rashidi et al. (2014b) presented the analytical solutions of transport phenomena in nanofluid adjacent to a nonlinearly porous stretching sheet. Sheikholeslami and Ganji (2013a) studied the heat transfer of Cu-water nanofluid flow between the parallel plates. Turkyilmazoglu (2013) studied the unsteady mixed convection flow of nanofluids over a moving vertical flat plate with heat transfer. Sheikholeslami et al. (2013b) determined free convection flow of nanofluid. Hayat et al. (2014) presented the mixed convection peristaltic flow of magnetohydrodynamic (MHD) nanofluid in presence of Brownian motion and thermophoresis. Casson fluid model is one of the base fluids which exhibits yield stress. However such fluid behaves like a solid when shear stress less than the yield stress is applied and it moves if applied shear stress is greater than yield stress. Examples of Casson fluid include jelly, soup, honey, tomato sauce, concentrated fruit juices, blood and many others. In fact several substances like protein, fibrinogen and globin in an aqueous base plasma, human red cells form a chain like structure, known as aggregates or rouleaux. If the rouleaux behaves like a plastic solid then there exists a field stress that can be identified with the constant yield stress in Casson fluid by Dash et al. (1996). Recently, Mukhopadhyay (2013a) provided the boundary layer flow of Casson fluid over a non-linearly stretching sheet. Some of the recent studies about flow of Casson fluid are [Shehzad et al. (2013), Mukhopadhyay and Vajravelu (2013b), Hayat et al. (2012a)].

Mixed convective flows along with thermal radiations are commonly encountered in many environmental and scientific developments, for instance, in aeronautics, fire research, heating and cooling of channels, etc. Thus it is of great worth to study the radiative convective flow. Makinde (2005) discussed the transient free convection interaction with thermal radiation of an absorbing emitting fluid along moving vertical permeable plate. Hayat et al. (2010) explored the MHD radiative mixed convection boundary layer stagnation point flow through a porous medium. No doubt the MHD flow has gained considerable interest due to its fundamental importance in the industrial and technological applications such as in coating of metals, crystal growth , electromagnetic pumps, MHD generators and reactor cooling. The Lorentz force interacts with the buoyancy force in governing the flow and temperature fields. The effect of Lorentz force is known to reduce the velocities. Heat and mass transfer characteristics in the magnetohydrodynamic (MHD) viscous flow over a permeable stretching surface is studied by Turkyilmazoglu (2011). Also Motsa et al. (2012) obtained the solutions for flow of upper- convected Maxwell fluid over porous stretching sheet in presence of magnetic field by using successive Taylor series linearization method.

In several natural processes the fluids experiencing exothermic or endothermic chemical reactions. Hence it is important to discuss the effects of heat source or sink. Occurrence of heat source or sink may change the temperature distribution in the fluid which disturbs the particle deposition rate in systems such as nuclear reactors, electronic chips, and semiconductor wafers. Hayat et al. (2012b) presented the radiative flow of Jeffery fluid in a porous medium with power law heat flux and heat source. Recently, Kandasamy et al. (2011) discussed the combined effect of thermal diffusion and diffusion thermo in free convective heat and mass transfer flow over a porous stretching surface in the presence of thermophoresis particle deposition and heat source/sink. The researchers at present are also very keen to discuss the significance of convective boundary conditions by Aziz (2009) in the flows under various aspects.

The present study deals with the convective boundary conditions in the mixed convection flow of nanofluid over a stretching sheet. Problem formulation is made in presence of thermal radiation, heat source/sink and first order chemical reaction. Casson fluid is taken as a base fluid. Boundary layer partial differential equations are reduced into set of ordinary differential equations by using appropriate transformations. Convergent solutions of the resulting problems are obtained by using homotopy analysis method [Liu et al. (2013), Hayat et al. (2013), Abbasbandy et al. (2013), Zheng et al. (2012), Rashidi et al. (2012b), Turkyilmazoglu (2012), Rashidi et al. (2014)].

Impacts of all embedding parameters are analyzed graphically for the temperature, concentration and flow fields. Numerical values of skin-friction coefficient, local Nusselt and Sherwood numbers for different parameters are calculated and analyzed.

2. MATHEMATICAL MODELING

Consider the mixed convection boundary layer flow of Casson nanofluid over a stretching surface with heat source/ sink. Flow is considered in presence of an applied magnetic field, thermal radiation and first order chemical reaction. Convective heat and mass conditions are taken at surface of the sheet. The rheological equation of state for an isotropic and incompressible flow of a Casson fluid is [12, 14, 15]:

$$\tau_{ij}=\begin{cases}2\left(\mu_B+p_y/\sqrt{2\pi}\right)e_{ij}, & \pi>\pi_c,\\ 2\left(\mu_B+p_y/\sqrt{2\pi_c}\right)e_{ij}, & \pi<\pi_c.\end{cases} \tag{1}$$

In above expression $\pi=e_{ij}e_{ij}$ and e_{ij} is the $(i,j)^{th}$ component of the deformation rate, π the product of the component of deformation rate with itself, π_c a critical value of this product based on the non-Newtonian model, μ_B the plastic dynamic viscosity of non- Newtonian fluid, and p_y the yield stress of fluid. The velocity field is taken as

$$\mathbf{V}=[u(x,y),v(x,y),0], \tag{2}$$

where u and v denote the velocity components in the x - and y -directions.

The governing equations for flow can be put into the forms:

$$\frac{\partial u}{\partial x}+\frac{\partial v}{\partial y}=0, \tag{3}$$

$$u\frac{\partial u}{\partial x}+v\frac{\partial u}{\partial y}=\nu\left(1+\frac{1}{\beta}\right)\frac{\partial^2 u}{\partial y^2}+g\beta_T(T-T_\infty)+g\beta_C(C-C_\infty)-\frac{\sigma^* B_0^2}{\rho}u, \tag{4}$$

$$u\frac{\partial T}{\partial x}+v\frac{\partial T}{\partial y}=\sigma\frac{\partial^2 T}{\partial y^2}-\frac{16\sigma_s T_\infty^3}{3k_e\rho c_p}\frac{\partial^2 T}{\partial y^2}+\frac{\rho^* c_p^*}{\rho c_p}\left(D_B\frac{\partial C}{\partial y}\frac{\partial T}{\partial y}+\frac{D_T}{T_\infty}\left(\frac{\partial T}{\partial y}\right)^2\right)+\frac{Q}{\rho c_p}(T-T_\infty), \tag{5}$$

$$u\frac{\partial C}{\partial x}+v\frac{\partial C}{\partial y}=D_B\frac{\partial^2 C}{\partial y^2}+\frac{D_T}{T_\infty}\frac{\partial^2 T}{\partial y^2}-k_1(C-C_\infty), \tag{6}$$

where β is the Casson fluid parameter, β_T the thermal expansion coefficient, β_C the concentration expansion coefficient, σ^* the electrical conductivity, B_0 the magnitude of applied magnetic field, ρ the density of fluid, g the gravitational acceleration, $\nu=(\mu_B/\rho)$ the kinematic viscosity, μ_B the dynamic viscosity, σ the thermal diffusivity, T the fluid temperature, σ_s the Stefan-Boltzmann constant, k_e the mean absorption coefficient, c_p the specific heat of fluid, ρ^* the density of nanoparticles, c^* the specific heat of nanoparticles, Q the uniform volumetric heat generation/absorption, C the concentration field and D_B the Brownian diffusion coefficient.

The boundary conditions can be expressed as follow:

$$\begin{aligned}&u=U_w(x)=cx,\ v=0,\\ &-k\frac{\partial T}{\partial z}=h(T_f-T),\\ &-D\frac{\partial C}{\partial z}=h^*(C_f-C)\ \text{at}\ y=0,\end{aligned} \tag{7}$$

$$u\to 0,\ v\to 0,\ T\to T_\infty,\ C\to C_\infty\ \text{as}\ y\to\infty, \tag{8}$$

where subscript w corresponds to the wall condition, h the heat transfer coefficient, h^* the concentration transfer coefficient, T_f the hot fluid temperature and C_f the hot fluid concentration. By using similarity transformations

$$\eta=y\sqrt{\frac{c}{\nu}},\ u=cxf'(\eta),v=-\sqrt{c\nu}\,f(\eta),\quad \theta(\eta)=\frac{T-T_\infty}{T_f-T_\infty},\ \varphi(\eta)=\frac{C-C_\infty}{C_f-C_\infty}, \tag{9}$$

equation (1) is identically satisfied and Eqs. (2)-(8) give:

$$(1+\frac{1}{\beta})f'''+ff''-(f')^2+\lambda(\theta+N\varphi)-Mf'=0, \tag{10}$$

$$(1+\frac{4}{3}R)\theta''+\Pr f\theta'+\Pr\left(N_b\theta'\varphi'+N_t\theta'^2\right)+\Pr\beta_1\theta=0, \tag{11}$$

$$\varphi''+Scf\varphi'+\frac{N_t}{N_b}\theta''-Sc\gamma\varphi=0, \tag{12}$$

$$f=0,\ f'=1,\ \theta'=-\gamma_1(1-\theta(0)),\ \varphi'=-\gamma_2(1-\varphi(0)),\ \text{at}\ \eta=0, \tag{13}$$

$$f'\to 0,\ \theta\to 0,\ \varphi\to 0\ \text{as}\ \eta\to\infty, \tag{14}$$

where λ is the mixed convection parameter, Gr_x the local Grashof number, N the concentration buoyancy parameter, M the Hartman number, R the radiation parameter, $\Pr$ the Prandtl number, N_b the Brownian motion parameter which is the irregular jiggling sort of movement exhibited by a small particle suspended in a fluid, N_t the thermophoretic parameter which is observed in mixtures of mobile particles where the different particle types exhibit different responses to the force of a temperature gradient, β_1 the heat

source/sink parameter, Sc the Schmidt number, γ the chemical reaction parameter, γ_1 the heat transfer Biot number and γ_2 the mass transfer Biot number. These can be defined in the forms

$$\lambda=\frac{Gr_x}{\mathrm{Re}_x^2},\ Gr_x=\frac{g\beta_T(T_f-T_\infty)x^3}{\upsilon^2},$$
$$N=\frac{\beta_C(C_w-C_\infty)}{\beta_T(T_f-T_\infty)},$$
$$R=(\frac{4\sigma^*T_\infty^3}{k_e k}),M=\frac{\sigma^*B_0^2}{\rho},$$
$$\mathrm{Pr}=\frac{\nu}{\sigma},N_b=\frac{\rho^*c^*D_B(C_w-C_\infty)}{\rho c\nu},\qquad(15)$$
$$N_t=\frac{\rho^*c^*D_T(T_w-T_\infty)}{\rho cT_\infty\nu},$$
$$\beta_1=\frac{Q}{\rho c_p},Sc=\frac{\nu}{D},\ \gamma=\frac{k_1}{c},$$
$$\gamma_1=\frac{h}{k}\sqrt{\frac{\nu}{a}},\ \gamma_2=\frac{h^*}{D}\sqrt{\frac{\nu}{a}}.$$

Non-dimensional local skin friction coefficient, local Nusselt and Sherwood numbers are

$$\frac{1}{2}C_f\,\mathrm{Re}_x^{1/2}=-\left(1+1/\beta\right)f''(0),\qquad(16)$$

$$Nu/\mathrm{Re}_x^{1/2}=-\theta'(0),\qquad(17)$$

$$Sh/\mathrm{Re}_x^{1/2}=-\varphi'(0),\qquad(18)$$

in which $\mathrm{Re}_x=\frac{cx}{\nu}$ is the local Reynold number.

3. SERIES SOLUTIONS

Initial guesses and auxiliary linear operators for series solutions are chosen in the forms

$$f_0(\eta)=\left(1-e^{-\eta}\right),\theta_0(\eta)=\frac{\gamma_1\exp(-\eta)}{1+\gamma_1},\qquad(19)$$
$$\varphi_0(\eta)=\frac{\gamma_2\exp(-\eta)}{1+\gamma_2},$$

$$L_f=f'''-f',\quad L_\theta=\theta''-\theta,L_\varphi=\varphi''-\varphi\qquad(20)$$

with the following properties

$$L_f(C_1+C_2e^{\eta}+C_3e^{-\eta})=0,$$
$$L_\theta(C_4e^{\eta}+C_5e^{-\eta})=0,\qquad(21)$$
$$L_\varphi(C_6e^{\eta}+C_7e^{-\eta})=0,$$

where $C_i\ \ (i=1-7)$ are the arbitrary constants.

Zeroth order deformation problems are

$$(1-p)L_f\left[\hat{f}(\eta;p)-f_0(\eta)\right]=p\hbar_f\mathbf{N}_f\left[\hat{f}(\eta;p),\hat{\theta}(\eta;p),\hat{\varphi}(\eta;p)\right]\qquad(22)$$

$$(1-p)L_\theta\left[\hat{\theta}(\eta;p)-\theta_0(\eta)\right]=p\hbar_\theta\mathbf{N}_\theta\left[\hat{f}(\eta;p),\hat{\theta}(\eta;p),\hat{\varphi}(\eta;p)\right]\qquad(23)$$

$$(1-p)L_\varphi\left[\hat{\varphi}(\eta;p)-\varphi_0(\eta)\right]=p\hbar_\varphi\mathbf{N}_\varphi\left[\hat{f}(\eta;p),\hat{\theta}(\eta;p),\hat{\varphi}(\eta;p)\right]$$

(24)

$$\hat{f}(0;p)=0,\ \hat{f}'(0;p)=1,\ \hat{f}'(\infty;p)=0$$
$$\hat{\theta}(\infty,p)=0,\hat{\theta}'(0,p)=-\gamma_1[1-\theta(0,p)]$$
$$\hat{\varphi}'(0,p)=-\gamma_2[1-\hat{\varphi}(0,p)],\ \hat{\varphi}(\infty,p)=0\qquad(25)$$

$$\mathbf{N}_f[\hat{f}(\eta;p),\hat{\theta}(\eta;p),\hat{\varphi}(\eta;p)]=\left(1+\frac{1}{\beta}\right)\frac{\partial^3\hat{f}(\eta,p)}{\partial\eta^3}+\hat{f}(\eta,p)\frac{\partial^2\hat{f}(\eta,p)}{\partial\eta^2}-\left(\frac{\partial\hat{f}(\eta,p)}{\partial\eta}\right)^2+\lambda\left(\hat{\theta}(\eta,p)+N\hat{\varphi}(\eta;p)\right)-M\frac{\partial\hat{f}(\eta,p)}{\partial\eta},\qquad(26)$$

$$\mathbf{N}_\theta[\hat{f}(\eta;p),\hat{g}(\eta;p),\hat{\theta}(\eta;p),\hat{\varphi}(\eta;p)]=\left(1+\frac{4}{3}R\right)\frac{\partial^2\hat{\theta}(\eta,p)}{\partial\eta^2}+\mathrm{Pr}(\hat{f}(\eta,p)\frac{\partial\hat{\theta}(\eta,p)}{\partial\eta}+\mathrm{Pr}\,N_b\frac{\partial\hat{\theta}(\eta,p)}{\partial\eta}\frac{\partial\hat{\varphi}(\eta,p)}{\partial\eta}+\mathrm{Pr}\,N_t\left(\frac{\partial\hat{\theta}(\eta,p)}{\partial\eta}\right)^2+\mathrm{Pr}\,\beta_1\hat{\theta}(\eta,p)\qquad(27)$$

$$\mathbf{N}_\varphi[\hat{f}(\eta;p),\hat{g}(\eta;p),\hat{\theta}(\eta;p),\hat{\varphi}(\eta;p)]=\frac{\partial^2\hat{\varphi}(\eta;p)}{\partial\eta^2}+Sc\hat{f}(\eta,p)\frac{\partial\hat{\varphi}(\eta;p)}{\partial\eta}+\frac{N_t}{N_b}\left(\frac{\partial^2\hat{\theta}(\eta,p)}{\partial\eta^2}\right)-Sc\gamma\hat{\varphi}(\eta;p),\qquad(28)$$

where p is an embedding parameter, $\hbar_f$, $\hbar_\theta$ and $\hbar_\varphi$ are the non-zero auxiliary parameters and $\mathbf{N}_f$, $\mathbf{N}_\theta$ and $\mathbf{N}_\varphi$ are the nonlinear operators. Taking $p=0$ and $p=1$ we have

$$\hat{f}(\eta;0)=f_0(\eta),\hat{\theta}(\eta,0)=\theta_0(\eta),\hat{\varphi}(\eta;0)=\varphi_0(\eta)$$
$$\hat{f}(\eta;1)=f(\eta),\hat{\theta}(\eta,1)=\theta(\eta),\ \hat{\varphi}(\eta;1)=\varphi(\eta).\qquad(29)$$

As p varies from 0 to 1 then $f(\eta,p)$, $\theta(\eta,p)$ and $\varphi(\eta,p)$ differ from $f_0(\eta)$, $\theta_0(\eta)$ and $\varphi_0(\eta)$ to $f(\eta)$, $\theta(\eta)$ and $\varphi(\eta)$. Using Taylor's expansion we obtain

$$f(\eta,p)=f_0(\eta)+\sum_{m=1}^{\infty}f_m(\eta)p^m,$$
$$f_m(\eta)=\frac{1}{m!}\frac{\partial^m f(\eta;p)}{\partial p^m}\bigg|_{p=0},\qquad(30)$$

$$\theta(\eta,p)=\theta_0(\eta)+\sum_{m=1}^{\infty}\theta_m(\eta)p^m,$$
$$\theta_m(\eta)=\frac{1}{m!}\frac{\partial^m\theta(\eta;p)}{\partial p^m}\bigg|_{p=0},\qquad(31)$$

$$\varphi(\eta, p) = \varphi_0(\eta) + \sum_{m=1}^{\infty} \varphi_m(\eta) p^m,$$

$$\varphi_m(\eta) = \frac{1}{m!} \frac{\partial^m \varphi(\eta; p)}{\partial p^m}\bigg|_{p=0}. \quad (32)$$

The convergence of above series strongly depends upon $\hbar_f$, $\hbar_g$, $\hbar_\theta$ and $\hbar_\varphi$. Considering that $\hbar_f$, $\hbar_\theta$ and $\hbar_\varphi$ are selected properly so that Eqs. (30) – (32) converge at $p=1$ therefore

$$f(\eta) = f_0(\eta) + \sum_{m=1}^{\infty} f_m(\eta), \quad (33)$$

$$\theta(\eta) = \theta_0(\eta) + \sum_{m=1}^{\infty} \theta_m(\eta), \quad (34)$$

$$\varphi(\eta) = \varphi_0(\eta) + \sum_{m=1}^{\infty} \varphi_m(\eta). \quad (35)$$

The final solution expressions can be expressed as follows:

$$f_m(\eta) = f_m^*(\eta) + C_1 + C_2 e^{\eta} + C_3 e^{-\eta}, \quad (36)$$

$$\theta_m(\eta) = \theta_m^*(\eta) + C_7 e^{\eta} + C_8 e^{-\eta}, \quad (37)$$

$$\varphi_m(\eta) = \varphi_m^*(\eta) + C_9 e^{\eta} + C_{10} e^{-\eta}, \quad (38)$$

where the special solutions are f_m^*, g_m^*, θ_m^* and φ_m^*.

4. CONVERGENCE ANALYSIS AND DISCUSSION

It is obvious that the series solutions $(33)-(35)$ consist of the auxiliary parameters $\hbar_f$, $\hbar_\theta$ and $\hbar_\varphi$. These auxiliary parameters are very important in order to adjust and control the convergence of the series solutions. We have sketched the $\hbar-$ curves at 18^{th} order of approximations to determine the convergence region where the $\hbar-$ curves become parallel to horizontal axis. Appropriate range of auxiliary parameters $\hbar_f$, $\hbar_\theta$ and $\hbar_\varphi$ are $-0.9 \le \hbar_f \le -0.25$, $-1.2 \le \hbar_\theta \le -0.2$ and $-1.2 \le \hbar_\varphi \le -0.10$ (see Fig.1). Figs. $(1a-1c)$ are drawn to predict the best values for auxiliary parameters. From these Figs. we noticed that the optimal values are $\hbar_f = \hbar_\theta = \hbar_\varphi = -0.7$. Table 1 concludes that the series solutions converge in the whole region of η when $\hbar_f = \hbar_\theta = \hbar_\varphi = -0.7$.

Effects of Casson fluid parameter β, Hartman number M, mixed convection parameter λ and concentration buoyancy parameter N on the velocity profile $f'(\eta)$ are analyzed in the Figs. 2-5. Fig. 2 reveals that the velocity profile $f'(\eta)$ and momentum boundary layer thickness decrease with an increase in Casson parameter β. Impact of Hartman number M on the velocity profile $f'(\eta)$ is displayed in Fig. 3. With an increase in M the velocity profile $f'(\eta)$ decreases.

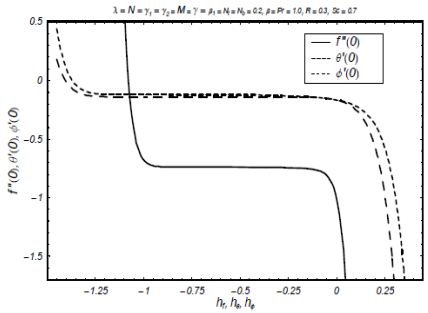

Fig. 1. H-curves for the function f(η), θ(η) and ϕ(η).

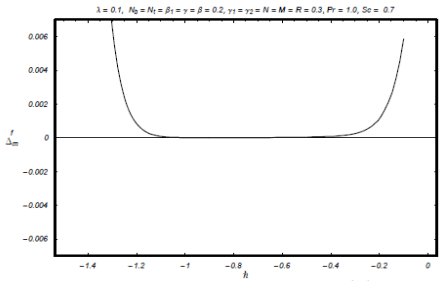

Fig. 1a. Residual error for f(η).

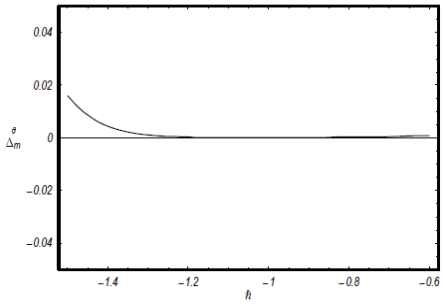

Fig. 1b. Residual error for θ(η).

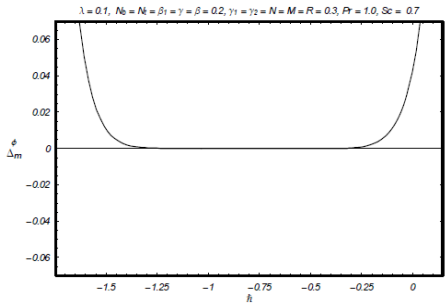

Fig. 1c. Residual error for ϕ(η).

Also momentum boundary layer thicknesses is a decreasing functions of M. This is due to the reason that with an increase in M the Lorentz force increases which resist the flow. Fig. 4 is plotted to analyze the influence of mixed convection parameter λ on the velocity profile $f'(\eta)$ in both assisting and opposing flows. It is observed that the velocity profile $f'(\eta)$ and momentum boundary layer thickness increase when $\lambda > 0$ (assisting flow) while opposite behavior is noted for $\lambda < 0$ (opposing flow).

Table 1 Convergence of series solutions for different order of approximations when $\beta = 0.5,\ \Pr = 1.0,\ Sc = 0.7,\ N_t = N_b = \beta_1 = \gamma = 0.2,$ $\lambda = N = M = R = \gamma_1 = \gamma_2 = 0.3$ and $\hbar_f = \hbar_\theta = \hbar_\varphi - 0.7.$

order of approximations	$-f''(0)$	$-\theta'(0)$	$-\varphi'(0)$
1	0.64200	0.21531	0.21408
5	0.62230	0.18139	0.19317
10	0.61302	0.16441	0.19295
15	0.60972	0.15770	0.19523
20	0.60859	0.15522	0.19657
25	0.60829	0.15450	0.19710
30	0.60828	0.15440	0.19722
35	0.60831	0.15446	0.19722
40	0.60831	0.15446	0.19722

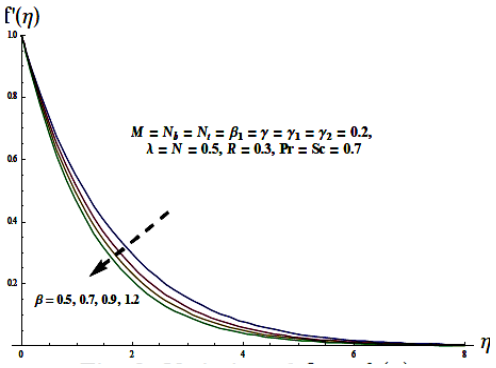

Fig. 2. Variation of β on *f*(η).

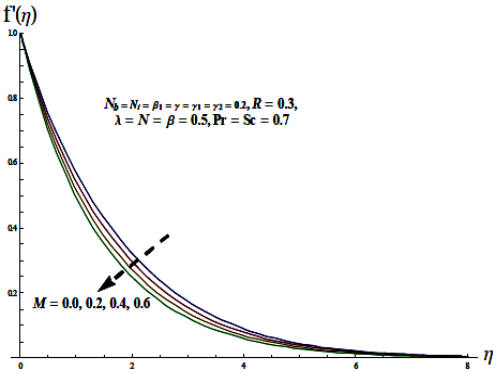

Fig. 3. Variation of *M* on *f*(η).

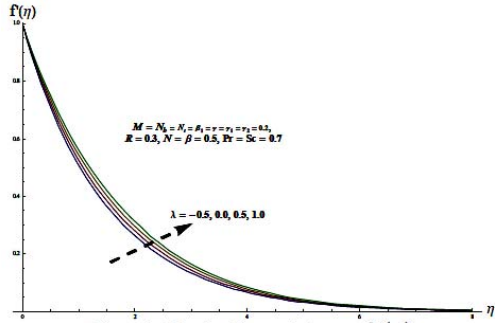

Fig. 4. Variation of λ on *f*(η).

It is examined that the momentum boundary layer thickness and velocity profile $f'(\eta)$ increase with an increase in N (see Fig. 5).

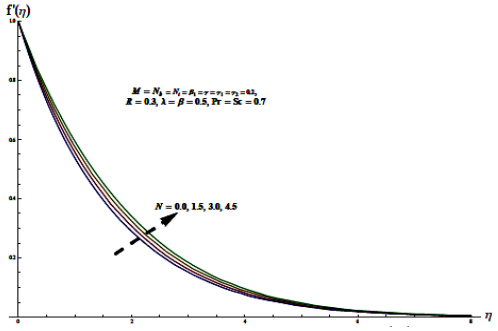

Fig. 5. Variation of *N* on *f*(η).

Figs. 6-16 are displayed to see the impacts of different parameters on the temperature $\theta(\eta)$ and concentration $\varphi(\eta)$. Figs. 6 and 7 show the variation of thermophoretic parameter N_t on the temperature $\theta(\eta)$ and concentration $\varphi(\eta)$. As thermophoresis causes the small particles to be driven away from a hot surface towards a cold one thats why temperature $\theta(\eta)$ and concentration profiles $\varphi(\eta)$ increase with an increase in thermophoretic parameter N_t.

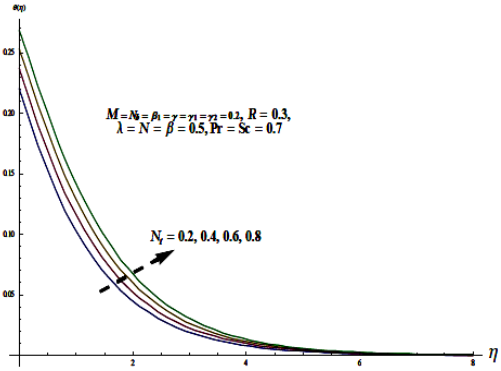

Fig. 6. Variation of N_t on θ(η).

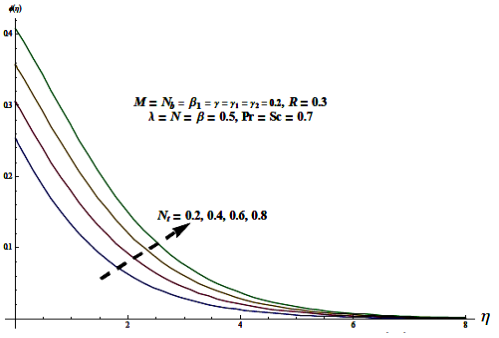

Fig. 7. Variation of N_t on θ(η).

Also the associated boundary layer thicknesses are increasing functions of N_t. Figs. 8 and 9 are plotted to see the variation of Brownian motion parameter N_b on the temperature $\theta(\eta)$ and concentration $\varphi(\eta)$. Thermal boundary layer

thickness and temperature $\theta(\eta)$ enhance when N_b increases. This is due to the reason that Brownian motion is a zig zag motion in which the kinetic energy of the particles increases which in results shows an increase in particle collision. It is also noticed that the concentration $\varphi(\eta)$ and associated boundary layer thickness reduces with an enhancement in N_b. Fig. 10 exhibits the effect of Prandtl number Pr on the temperature $\theta(\eta)$. Both conduction and convection happen in fluids. As heat transfer through both processes reduces the temperature difference, they can be considered as competing against each other in transferring heat. There are many different types of fluids, such as air, water, oil, or mercury. The rates of conduction and convection vary in different fluids. Sometimes, conduction dominates. Other times, convection dominates. The Prandtl number is a parameter that can be used to roughly determine which process will win.

As Pr is inversely proportional to thermal diffusivity so due to an increase in Pr the thermal diffusivity decreases which reduces both the thermal boundary layer thickness and temperature $\theta(\eta)$. Variation of Schmidt number Sc on the concentration profile $\varphi(\eta)$ is seen in Fig. 11. With an increase in Sc the mass diffusivity reduces which in turn decreases the concentration boundary layer thickness. Influence of heat source/sink parameter β_1 on the temperature $\theta(\eta)$ is analyzed in Fig. 12. Thermal boundary layer thickness and temperature $\theta(\eta)$ are increasing functions of $\beta_1 > 0$ (internal heat source) while reverse is observed in case of $\beta_1 < 0$ (internal heat sink).

Fig. 13 is designed to see the influence of thermal radiation R on the temperature $\theta(\eta)$. It is noticed that temperature $\theta(\eta)$ enhances due to an increase in radiation parameter R.

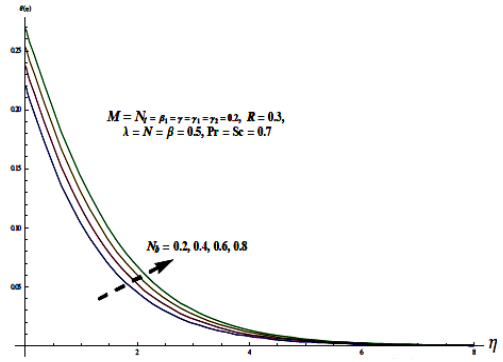

Fig. 8. Variation of N_b on θ(η).

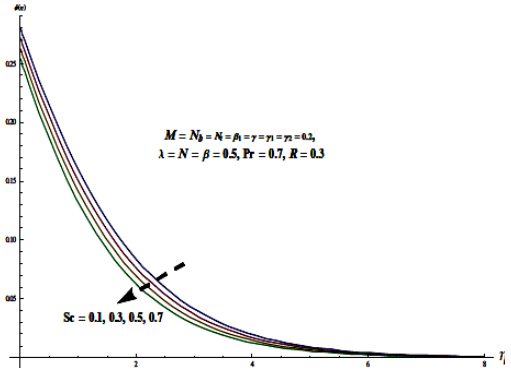

Fig. 11. Variation of Sc on θ(η).

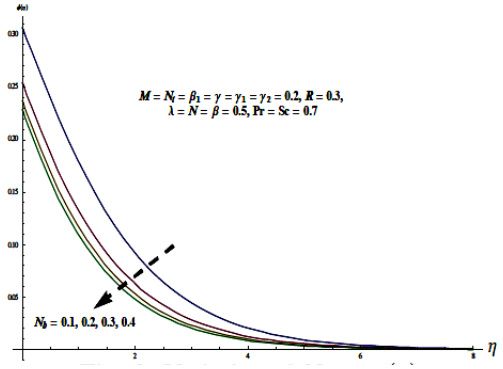

Fig. 9. Variation of N_b on ϕ(η).

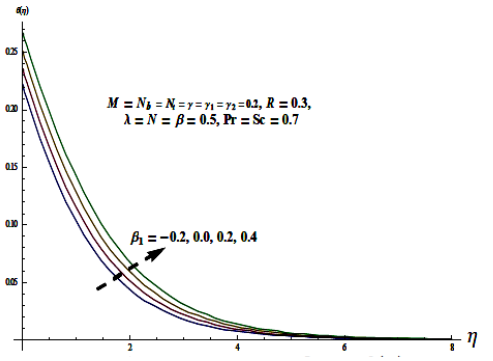

Fig. 12. Variation of β_1 on ϕ(η).

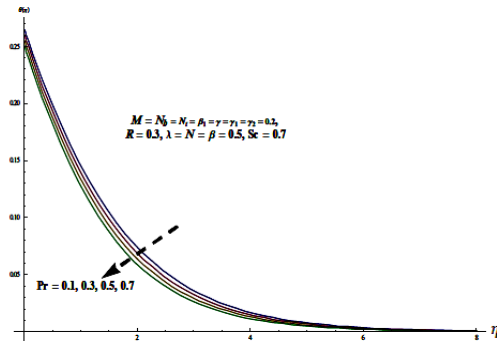

Fig. 10. Variation of Pr on θ(η).

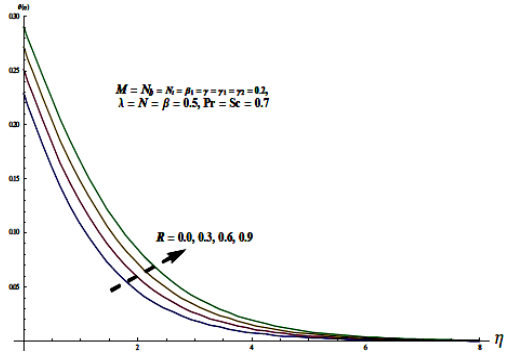

Fig. 13. Variation of R on θ(η).

It is because of the fact that for larger R the mean absorption coefficient k_e decreases which enhances the divergence of the radiative heat flux. Hence, the rate of radiative heat transfer to the fluid will rise and consequently the fluid temperature increases. Figs. 14 and 15 are drawn to see the effects of heat transfer Biot number γ_1 and mass transfer Biot number γ_2 on the temperature $\theta(\eta)$ and concentration $\varphi(\eta)$ respectively. With an enhancement in heat transfer Biot number γ_1 , the thermal boundary layer thickness and temperature $\theta(\eta)$ increase. Also the associated boundary layer and concentration $\varphi(\eta)$ are increasing functions of mass transfer Biot number γ_2.

Fig. 16 exhibits the effect of generative/destructive chemical reaction γ on the concentration $\varphi(\eta)$. It is found that the associated boundary layer thickness and concentration profile $\varphi(\eta)$ enhance with generative chemical reaction ($\gamma < 0$) while opposite behavior is noted for destructive chemical reaction ($\gamma > 0$) .

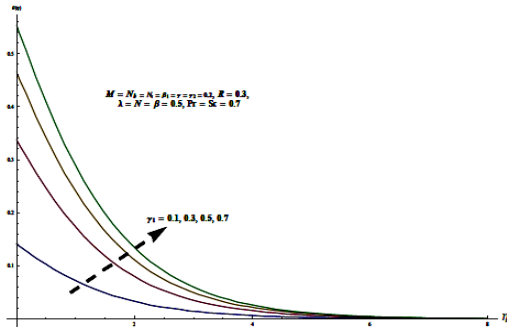

Fig. 14. Variation of γ_1 on θ(η).

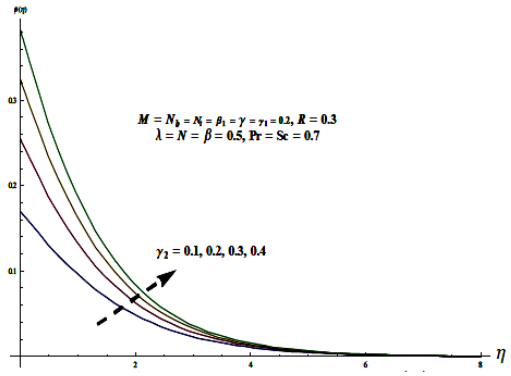

Fig. 15. Variation of γ_2 on θ(η).

Tables 2-4 are prepared to explore the impacts of Casson fluid parameter β, thermophoretic parameter N_t, Brownian motion parameter N_b , mixed convection parameter λ, concentration buoyancy parameter N , heat transfer Biot number γ_1 and mass transfer Biot number γ_2 on skin-friction coefficient and local Nusselt and Sherwood numbers. With an enhancement in N_t and β , the Skin-friction coefficient and local Nusselt and Sherwood numbers decrease. Also with an increase in γ_1 and N_b the skin-friction coefficient and Sherwood number increases while local Nusselt number reduces. In case of assisting flow ($\lambda > 0$) and with an enhancement in N, the local Nusselt and Sherwood numbers enhance. The skin-friction coefficient reduces while reverse is the impact in case of opposing flow ($\lambda < 0$). Sherwood number rises with an increase in mass transfer Biot number γ_2 while skin-friction coefficient and local Nusselt number decrease with an increase in γ_2.

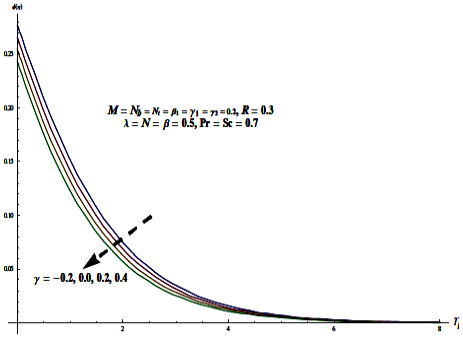

Fig. 16. Variation of γ on θ(η).

Table 2 Numerical values of local Nusselt number $-\theta'(0)$ and Sherwood number $-\varphi'(0)$ for different values of parameters β, N_t, N_b when

$\beta_1 = R = M = 0.0, \lambda = N = 0.3, \gamma_1 = \gamma_2 = 0.2,$
$\Pr = 1.0,\ Sc = 0.7$ **and** $\hbar_f = \hbar_\theta = \hbar_\varphi - 0.7$.

β	N_t	N_b	$-\theta'(0)$	$-\varphi'(0)$
0.5	0.2	0.2	0.15271	0.12054
0.7			0.15204	0.11910
0.9			0.15150	0.11758
0.5	0.2		0.15271	0.12054
	0.4		0.15195	0.096142
	0.6		0.15106	0.071520
0.5	0.2	0.2	0.15271	0.12054
		0.4	0.15186	0.13368
		0.6	0.15100	0.13815

CONCLUSIONS

The present investigation discusses the mixed convection flow of nanofluid over a stretching surface in presence of heat source/ sink and first order chemical reaction. Main findings of present study are mentioned below.

a) Momentum boundary layer thickness and velocity profile $f'(\eta)$ enhance with the increase in β and M while these are reduced via N .

b) In case of assisting flow $\lambda > 0$ both the velocity profile $f'(\eta)$ and momentum boundary layer thickness shoot up while reverse behavior is observed in case of

opposing flow $\lambda < 0$.

c) With an enhancement in thermophoretic parameter N_t the temperature $\theta(\eta)$ and concentration profiles $\varphi(\eta)$ increase.

d) Influence of Brownian motion parameter N_b on the thermal boundary layer thickness and temperature $\theta(\eta)$ is qualitatively opposite to that of concentration boundary layer thickness and concentration profile $\varphi(\eta)$.

e) Thermal boundary layer thickness reduces with an increase in Prandtl number Pr and internal absorption parameter $\beta_1 < 0$ while it increases with the increase in thermal radiation R, internal heat generation $\beta_1 > 0$ and heat transfer Biot number γ_1.

f) Concentration profile $\varphi(\eta)$ and associated boundary layer thickness are increasing functions of mass transfer Biot number γ_2 and generative chemical reaction $\gamma < 0$ while reverse behavior is noted for Schmidt number Sc and destructive chemical reaction $\gamma > 0$.

g) Skin-friction coefficient and local Nusselt and Sherwood numbers reduce through enhancement in Casson fluid parameter β and thermophoretic parameter N_t.

h) Rise in Brownian motion parameter N_b increases the skin-friction coefficient and Sherwood number while it decreases the local Nusselt number.

i) In assisting flow $\lambda > 0$ the skin-friction coefficient decreases while opposite behaviors found for opposing flow $\lambda < 0$.

Table 3 Numerical values of local Nusselt number $-\theta'(0)$ and Sherwood number $-\varphi'(0)$ for different values of parameters γ_1, γ_2, λ, N when $\beta_1 = R = M = 0.0, N_t = N_b = 0.2,$ $\beta = 0.5, \Pr = 1.0,\ Sc = 0.7$ and $\hbar_f = \hbar_\theta = \hbar_\varphi - 0.7$

λ	N	γ_1	γ_2	$-\theta'(0)$	$-\varphi'(0)$
-0.5	0.3	0.2	0.2	1.5201	0.11969
0.0				0.15248	0.12014
0.3				0.15271	0.12054
0.6				0.15302	0.12144
0.3	0.0			0.15261	0.12032
	0.3			0.15271	0.12054
	0.6			0.15302	0.12078
0.3	0.3	0.2		0.15271	0.12054
		0.4		0.24602	0.10535
		0.6		0.30822	0.095273
0.3	0.3	0.2	0.1	0.15304	0.069638
			0.3	0.15255	0.15995
			0.5	0.15224	0.21584

j) Enhancement in concentration buoyancy parameter N, heat transfer Biot number γ_1 and mass transfer Biot number γ_2 reduces the skin-friction coefficient.

k) Local Nusselt and Sherwood numbers are increasing functions in case of assisting flow $\lambda > 0$ and decreasing functions for opposing flow $\lambda < 0$.

Table 4 Numerical values of skin-friction coefficient $-\left(1+\frac{1}{\beta}\right) f''(0)$ for different values of parameters β, N_t, N_b, γ_1, γ_2, λ, N when $\beta_1 = R = M = 0.0, \Pr = 1.0,\ Sc = 0.7$ and $\hbar_f = \hbar_\theta = \hbar_\varphi - 0.7.$

β	N_t	N_b	λ	N	γ_1	γ_2	$-\left(1+\frac{1}{\beta}\right) f''(0)$
0.5	0.2	0.2	0.3	0.3	0.2	0.2	1.6532
0.7							1.4797
0.9							1.3741
0.5	0.2						1.6532
	0.4						1.6368
	0.6						1.6204
0.5	0.2	0.2					1.6532
		0.4					1.6598
		0.6					1.6613
0.5	0.2	0.2	-0.5	0.3	0.2	0.2	1.8689
			0.0				1.7321
			0.3				1.6532
			0.6				1.5770
			0.3	0.0			1.6863
				0.3			1.6532
				0.6			1.6207
0.5	0.2	0.2	0.3	0.3	0.2		1.6532
					0.4		1.6152
					0.6		1.5893
0.5	0.2	0.2	0.3	0.3	0.2	0.1	1.6598
						0.3	1.6484
						0.5	1.6413

Also the associated boundary layer thicknesses are increasing functions of N_t.

ACKNOWLEDGEMENT

The suggestions of reviewer regarding an earlier version are appreciated.

REFERENCES

Abbasbandy, S., M. S. Hashemi and I. Hashim (2013). On convergence of homotopy analysis method and its application to fractional integro-differential equations. *Quaestiones Mathematicae* 36(1), 93-105.

Alsaedi, A., M. Awais and T. Hayat (2012). Effects of heat generation/absorption on stagnation point flow of nanofluid over a surface with convective boundary conditions. *Communications in Nonlinear Science and Numerical Simulation* 17(11), 4210-4223.

Aziz, A. (2009). A similarity solution for laminar thermal boundary layer over a flat plate with a convective surface boundary condition. *Communications Nonlinear Science and Numerical Simulation* 14(4), 1064-1068.

Buongiorno, J. (2006). Convective transport in nanofluids. *Journal of Heat Transfer* 128(3), 240-250.

Choi, S. (1995). Enhancing thermal conductivity of fluids with nanoparticles. *Developments and Applications of non-Newtonian Flows* 66,.99-105.

Dash, R. K., K. N. Mehta and G. Jayaraman (1996). Casson fluid flow in a pipe filled with a homogeneous porous medium. *International Journal of Engineering Science* 34 (10), 1145-1156.

Hayat, T., S. A. Shehzad, A. Alsaedi and M. S. Alhothuali (2012a). Mixed convection stagnation point flow of Casson fluid with convective boundary conditions. *Chinise Physics Letter* 29(11) 114704.

Hayat, T., F. M. Abbasi, M. A. Yami and S. Monaque (2014). Slip and Joule heating effects in mixed convection peristaltic transport of nanofluid with Soret and Dufour effects. *Journal of Molecular Liquids* 194(2014), 93-99.

Hayat, T., S. A. Shehzad, M. B. Ashraf and A. Alsaedi (2013). Magnetohydrodynamic mixed convection flow of thixotropic fluid with thermophoresis and Joule heating. *Journal of Thermophysics and Heat Transfer* 27, 733-740.

Hayat, T., S. A. Shehzad, M. Qasim and S. Obaidat (2012b). Radiative flow of Jeffery fluid in a porous medium with power law heat flux and heat source. *Nuclear Engineering and Design* 243, 15-19.

Hayat, T., Z. Abbas, I. Pop and S. Asghar (2010). Effects of radiation and magnetic field on the mixed convection stagnation-point flow over a vertical stretching sheet in a porous medium. *International Journal of Heat and Mass Transfer* 53(1-3), 466-474.

Kandasamy, R., T. Hayat and S. Obaidat (2011). Group theory transformation for Soret and Dufour effects on free convective heat and mass transfer with thermophoresis and chemical reaction over a porous stretching surface in the presence of heat source/sink. *Nuclear Engineering and Design* 241, 2155-2161.

Liu, Y.P., S. J. Liao and Z. B. Li (2013). Symbolic computation of strongly nonlinear periodic oscillations. *Journal of Symbolic Computation* 55, 72-95.

Makinde, O. D. (2005). Free convection flow with thermal radiation and mass transfer past a moving vertical porous plate. International *Communications in Heat and Mass Transfer* 32(10), 1411-1419.

Masuda, H., A. Ebata, K. Teramae and N. Hishinuma (1993). Alteration of thermal conductivity and viscosity of liquid by dispersing ultra-fine particles. Dispersion of Al2O3, SiO2 and TiO2 Ultra-Fine Particles. *Netsu Bussei* 7(4), 227-233.

Motsa, S. S., T. Hayat and O. M. Aldossary (2012). MHD flow of upper- convected Maxwell fluid over porous stretching sheet using successive Taylor series linearization method. *Applied Mathematics and Mechanics* 33(8), 975-990.

Mukhophadhyay, S. (2013a). Casson fluid flow and heat transfer over a nonlinearly stretching surface. *Chinise Physics* B 22(7), 074701.

Mukhophadhyay, S. and K. Vajravelu (2013b). Diffusion of chemically reactive species in Casson fluid flow over an unsteady permeable stretching surface. *Journal of Hydrodynamics* 25(4), 591-598.

Mustafa, M., T. Hayat and A. Alsaedi (2013). Unsteady boundary layer flow of nanofuid past an impulsively stretching sheet. *Journal of Mechanics* 29(3), 423-432.

Rashidi, M. M., N. F. Mehr, A. Hosseini, O. A. Bég and T. K. Hung (2014a). Homotopy simulation of nanofluid dynamics from a non-linearly stretching isothermal permeable sheet with transpiration. *Meccanica* 49(2), 469-482.

Rashidi, M. M., N. Kavyani and S. Abelman (2014b). Investigation of entropy generation in MHD and slip flow over a rotating porous disk with variable properties. *International Journal of Heat and Mass Transfer* 70, 892-917.

Rashidi, M. M., O. A. Bég, N. F. Mehr, A. Hosseini and R. S. R. Gorla (2012a). Homotopy simulation of axisymmetric laminar mixed convection nanofluid boundary layer over a vertical cylinder. *Theoretical and Applied Mechanics* 39(4), 365-390.

Rashidi, M. M., S.C. Rajvanshi and M. Keimanesh (2012b). Study of Pulsatile flow in a porous annulus with the homotopy analysis method. *International Journal of Numerical Methods for Heat & Fluid Flow* 22(8), 971-989.

Shehzad, S. A., T.Hayat, M. Qasim and S. Asghar (2013). Effects of mass transfer on MHD flow of a Casson fluid with chemical reaction and suction. *Brazilian Journal of Chemical Engineering* 30(1), 187-195.

Sheikholeslami, M. and D. D. Ganji (2013a). Heat transfer of Cu-water nanofluid flow between parallel plates. *Powder Technology* 235, 873-879.

Sheikholeslami, M., M. G. Bandpy and G. Domairry (2013b). Free convection of nanofluid filled enclosure using lattice Boltzmann method (LBM). Applied *Mathematics and Mechanics* 34(7), 833-846.

Turkyilmazoglu, M. (2011). Analytic heat and mass transfer of the mixed hydrodynamic/thermal slip MHD viscous flow over a stretching sheet. *International Journal Of Mechanical Sciences* 53(10), 886-896.

Turkyilmazoglu, M. (2012). Solution of Thomas-Fermi equation with a convergent approach . *Communications Nonlinear Science and Numerical Simulation* 17(11), 4097-4103.

Turkyilmazoglu, M. (2013). Unsteady convection flow of some nanofluids past a moving vertical flat plate with heat transfer. *Journal of Heat Transfer* 136(3), 031704.

Zheng, L., J. Niu, X. Zhang and Y. Gao (2012). MHD flow and heat transfer over a porous shrinking surface with velocity slip and temperature jump. *Mathematical and Computer Modelling* 56(5-6), 133-144.